PAPER • **OPEN ACCESS**

Remote sensing of surface Hydrothermal Alteration, identification of Minerals and Thermal anomalies at Sveifluháls-Krýsuvík high-temperature Geothermal field, SW Iceland

To cite this article: Lucía Magali Ramírez-González *et al* 2019 *IOP Conf. Ser.: Earth Environ. Sci.* **254** 012005

View the article online for updates and enhancements.

IOP ebooks™

Bringing you innovative digital publishing with leading voices to create your essential collection of books in STEM research.

Start exploring the collection - download the first chapter of every title for free.

This content was downloaded from IP address 89.17.138.178 on 08/09/2019 at 23:06

Remote sensing of surface Hydrothermal Alteration, identification of Minerals and Thermal anomalies at Sveifluháls-Krýsuvík high-temperature Geothermal field, SW Iceland

Lucía Magali Ramírez-González[1], Muhammad Aufaristama[1], Ingibjörg Jónsdóttir[1], Ármann Höskuldsson[1], Þorvaldur Þórðarson[1], Nicolas Marino Proietti[2], Gilles Kraft[2] and Jamie McQuilkin[2]

[1] Institute of Earth Sciences, University of Iceland, Askja-Sturlugata 7, 101 Reykjavík
[2] ReSource International ehf., Hliðasmári 2, 201 Kopavogur, Iceland

Email: maga.ramglez@gmail.com

Abstract. This study used optical remote sensors to identify surface hydrothermal alteration and thermal anomalies in Krýsuvík geothermal field. Multispectral Landsat and ASTER satellite images were used to identify hydrothermal alteration minerals and thermal anomalies. A hyperspectral image from Hyperion was used for the analysis of absorption features. Spectral analysis from the visible (VIS) to the short wavelength infrared (SWIR) allowed the identification of possible sulfur, iron oxides, and montmorillonite. A time series analysis of thermal anomalies using the nighttime satellite images from 2002 to 2017 detected extinct surface hydrothermal activity southwest of the study area, and a thermal anomaly possibly affected by crustal deformation in the southeast. In Seltún area, thermal infrared (TIR) images acquired by a camera on an unmanned aerial vehicle (UAV) were compared with ground measurements; the aim was assessing the accuracy of the TIR images regarding the distance between the camera and the ground. The TIR image taken at 30 m elevation was used to calculate radiative heat flux; values were in same order of magnitude than the heat flux through the soil estimated by using ground measurements. This study provides insights for monitoring natural or induced changes on the surface geothermal activity of geothermal fields.

1. Introduction

The Krýsuvík high-temperature geothermal field is located in a central part of Reykjanes peninsula, in the southwest of Iceland. Krýsuvík belongs to a volcanic fissure swarm which subglacial volcanism during the late Pleistocene produced long hyaloclastite ridges arranged in echelons at approximately 45˚NE [1]. The main surface activity is confined to the southeast of the Sveifluháls ridge, mostly within the areas of Seltún and Hveradalir, areas characterized by intensive surface alteration, steam vents, mud pots and hot springs. A simplified geothermal map of the study area is shown in Figure 1.

Content from this work may be used under the terms of the Creative Commons Attribution 3.0 licence. Any further distribution of this work must maintain attribution to the author(s) and the title of the work, journal citation and DOI.
Published under licence by IOP Publishing Ltd

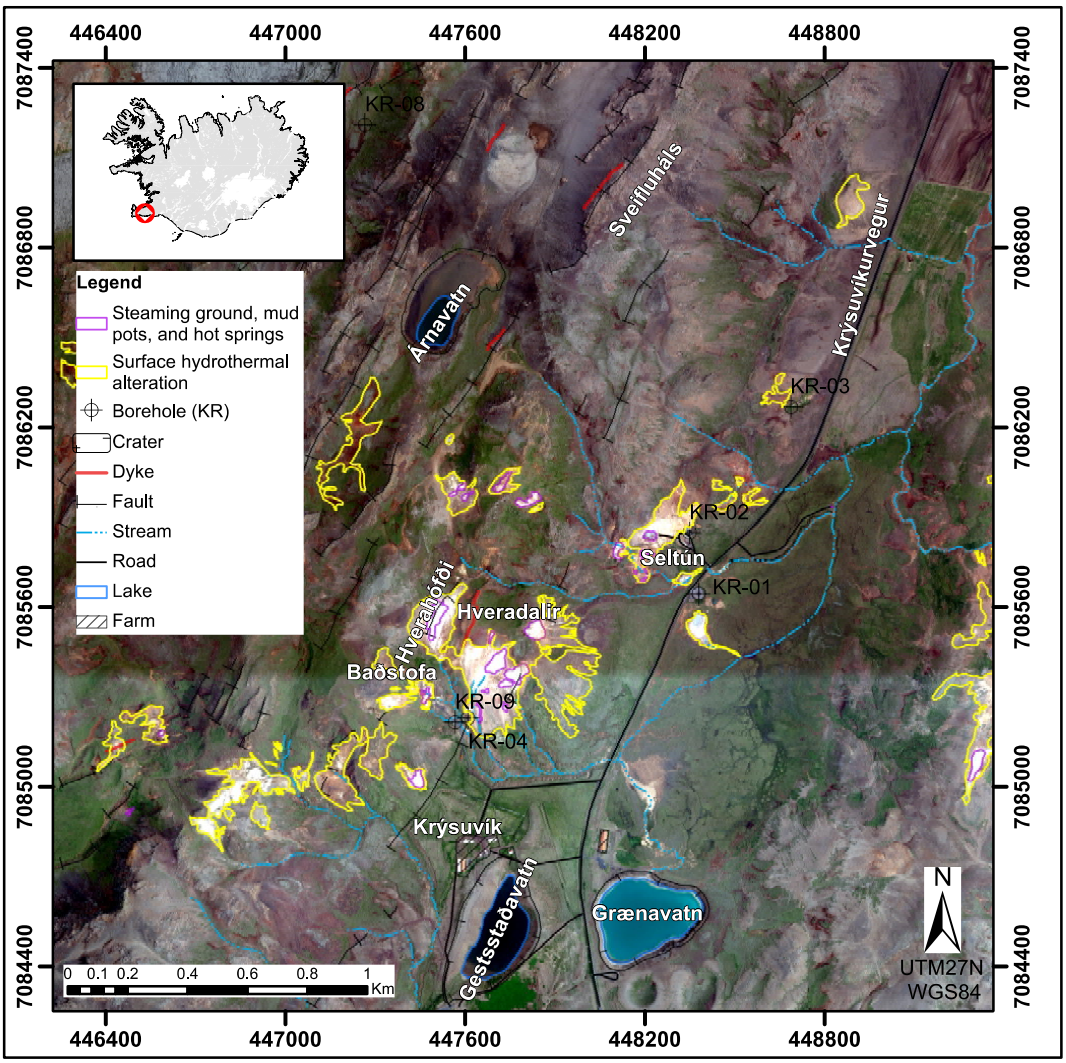

Figure 1. Simplified geothermal map of Sveifluháls. The mapping of surface alteration used aerial photographs [2]. Faults and dykes were mapped taking as reference previous geothermal maps [3][4][5].

The objective of this study was to identify hydrothermal alteration minerals and thermal anomalies in Sveifluháls by using optical remote sensors. We use multispectral and hyperspectral satellite images, and thermal infrared (TIR) images acquired by a camera mounted on an unmanned aerial vehicle (UAV) also called drone.

The combination of processing techniques, spectral and spatial resolution of the sensors, as well as the time range of the images acquisition, allowed regional and local analysis of the surface activity of the area that led to identify areas where the surface geothermal activity has changed over the time.

2. Data and methodology

2.1. Data

Spectral signatures of alteration minerals were identified by using multispectral satellite images from Landsat and ASTER, and one hyperspectral image from Hyperion. The satellite images were selected avoiding as much as possible clouds coverage. Landsat and ASTER were also used for identifying thermal anomalies; nighttime images (satellite in ascending mode) were chosen in order to avoid the

solar contribution. The acquisition date of the satellite images is shown in Table 1. The satellite images were downloaded as GeoTIFF files from the USA Geological Survey (USGS) EarthExplorer webpage.

For surveying, a TIR camera (7.5-13.5 μm) Zenmuse XT by FLIR was mounted on a UAV DJI Inspire 1 V2.0. TIR images were taken over the same target at 10m intervals, from 10 to 100 m. For comparison and further calibration of the TIR images, ground temperature measurements over the area covered by the TIR images were taken by using a type-K thermocouple temperature probe. Measurements were taken in soil at 1cm, 5 cm, and 12.5 cm deep, and also in the water and surrounding mud of the fumaroles covered by the images. GPS coordinates were taken for each point.

Table 1. List of satellite images used for this study. Data were downloaded from the USGS EarthExplorer.

Platform - Satellite	Acquisition date	Mapping purpose
Landsat 7 ETM+	March 26th, 2002 (nighttime scene)	Thermal anomalies
Landsat 7 ETM+	September 28th, 2003 (nighttime scene)	
Terra - ASTER	September 22nd, 2010 (nighttime scene)	
Terra - ASTER	October 27th, 2011 (nighttime scene)	
Terra - ASTER	November 12th, 2011 (nighttime scene)	
Terra - ASTER	November 1st, 2013 (nighttime scene)	
Landsat 8 OLI&TIRS	February 15th, 2014 (nighttime scene)	
Landsat 8 OLI&TIRS	April 23rd, 2015 (nighttime scene)	
Landsat 8 OLI&TIRS	July 30th, 2016 (nighttime scene)	
Landsat 8 OLI&TIRS	August 18th, 2017 (nighttime scene)	
Landsat 5 TM	September 15th, 1998	Hydrothermal alteration minerals
Terra – ASTER	June 26th, 2007	
EO1 – Hyperion	December 2nd, 2010	
Landsat 8 OLI&TIRS	July 30th, 2016	

The flight using the TIR camera by the UAV was carried out by the company ReSource International on November 1, 2017, between 17:00 and 17:30 hrs. (after the sunset during fall). The direct ground measurements were taken immediately after the flight.

Geographically, all data were projected using Universal Transverse Mercator (UTM) projection zone 27 North, and the World Geodetic System (WGS) 1984 as geographic coordinate system, datum and spheroid. ENVI® 5.1 software was used mainly for processing and ArcGIS® 10.4.1 for georeferencing and displaying.

2.2. Methodology

2.2.1. Pre-processing. Daytime Landsat and ASTER images were used for mineral identification. The images were radiometrically calibrated by using the radiometric calibration module of ENVI® 5.1. To obtain the surface reflectance filtrating the scattered radiation by the atmosphere; the dark-object technique [6] from ENVI® 5.1 was used. After this, the visible and near infrared (VNIR) bands of ASTER (band 1,2 and 3) were resized from 15m to 30m for further processing.

For thermal analysis, the nighttime Landsat and ASTER images were radiometrically calibrated and then atmospherically corrected for atmospheric up-welling radiation and atmospheric attenuation in ENVI® 5.1.

The hyperspectral image from Hyperion was used for mineral identification. 81 bands from the total of 242 bands were used. Uncalibrated bands, bands with water absorption and with strong vertical striping were avoided. The atmospheric calibration was performed by using the FLAASH® (Fast Line-of-sight Atmospheric Analysis of Spectral Hypercubes) module included in ENVI® 5.1.

The TIR images acquired by the UAV were converted to absolute temperature by multiplying the counts by the scale factor of 0.04 (according to the Zenmuse XT specifications). For georeferencing the thermal images, GPS coordinates were taken at known reference points and used to create links to the images. The georeferencing process was executed in ArcGIS® 10.4.1 by using the adjust transformation.

2.2.2. Identification of minerals. As first approach to identify areas of hydrothermal alteration, the spectral bands of Landsat and ASTER were used to form false colour images by applying band combinations. The band ratio technique was used to identify spectral signatures of specific minerals. The chosen bands for the band ratios classification technique have to have contrasting responses within the absorption features of the reflectance curve of the target mineral or group of minerals. For that, target minerals were taken as reference from a summary of alteration minerals in Krýsuvík identified by a previous geochemistry study [7]. Those minerals were: kaolinite, montmorillonite, hematite, goethite, anatase, pyrite, gypsum, covellite, anhydrite, antlerite, amorphous silica, antigorite, and native sulfur.

The multispectral images were also analyzed by the principal component analysis (PCA). The PCA was performed according to the Crosta technique which allows the identification of iron oxides (F) and hydroxyl (H) [8] by locating the PCs with the eigenvectors most influential in the absorption and reflectance of F and H minerals.

The hyperspectral image Hyperion, was used to analyse absorption wavelength position and depth following the simple linear approximation method of the absorption features parameters [9]. The absorption features were analysed by using the continuum-removed spectrum of each pixel into DISPEC 3.2.

2.2.3. Identification of thermal anomalies. The kinetic land surface temperature (LST) was retrieved from Landsat and ASTER nighttime images by using the emissivity normalization method [10] executed in ENVI® 5.1. The constant emissivity value was 0.95 (mean for basalts). The kinetic LST corresponds to the integrated temperature over the pixel size of 30x30 m for Landsat and 90 x 90 m for ASTER. It was calculated for the ten images used for thermal mapping in this study. In order to normalize the results, the thermal anomalies were categorized according to standard deviations (SD) above the background (BG) temperature.

2.2.4. Heat flux estimation. The TIR images taken by the UAV were used for heat loss calculations over Seltún on an area with warm ground and fumaroles. For those conditions, heat losses can be related to conduction trough the soil and radiation. Because of from the thermal images we can just obtain the surface temperature, the only heat loss mechanism taking into account was radiation. The radiation heat loss was obtained using the Stefan-Boltzman law, equation (1):

$$H_r = A\varepsilon\sigma \left(T_P^4 - T_{ATM}^4\right) \quad (1)$$

Where A is the area of the pixel in m^2, ε is the emissivity constant (0.95), σ is the Stefan-Boltzman constant (5.68 x 10^{-8} J/sm^2), T_P is the pixel temperature value in Kelvin, and T_{ATM} is the air temperature in Kelvin (275.05 K at the moment of the flight). Calculations were executed in the band math of ENVI® 5.1.

For comparison, the direct ground temperature measurements were used to estimate the heat flux density through the soil by using the method of Dawson (1964) [11], equation (2). This method was initially calibrated at the Wairakai geothermal field at New Zealand, and used for heat flux estimation through soil in Reykjanes geothermal area [12].

$$q_s = 5.2 \times 10^{-6}\, t_{15}^{4} \quad (2)$$

This method uses t_{15} that corresponds to the soil temperature at 15 cm depth (in degrees Celsius). For this study, the maximum depth measured in the soil was 12.5 cm, thus, the results were proportionally adapted to this depth.

3. Results and discussion

For easier analysis, it is suggested to focus the attention within the geothermal areas of Seltún and Hveradalir. The areas of surface geothermal alteration were identified first by using aerial photographs [2] and then by band combinations of the multispectral images. The 5,6,7 false color image using Landsat 8, and 9,2,4 for ASTER shown good contrast.

The results of the band ratios technique are shown in Figure 2. The map corresponds to a RGB false color composite using 6/7, 6/5, 2/1 band ratios of Landsat 8 from July 30, 2016. Taking as reference the target minerals, the ratios can be interpreted as: high 2/1 as possible sulfur, anatase and covellite; high 6/7 as possible montmorillonite, kaolinite and antigorite; and high 6/5 as possible hematite and goethite. The RGB composite has to be interpreted by taking into account the reflectance curve of the target minerals and the RGB additive theory of colors. In this way, magenta colors that are formed with red and blue represent areas where the ratios 6/7 and 2/1 have large values. The yellow colors, formed with red and green, represent high 6/7 and 6/5 ratios. The bright white colors represent areas where the three ratios have large values. As it can be noticed, high 6/7 ratio (interpreted as kaolinite and montmorillonite) seems to be widely spread within the geothermal area. Outside the geothermal area, the red colors represent vegetation and the green the unaltered rocks.

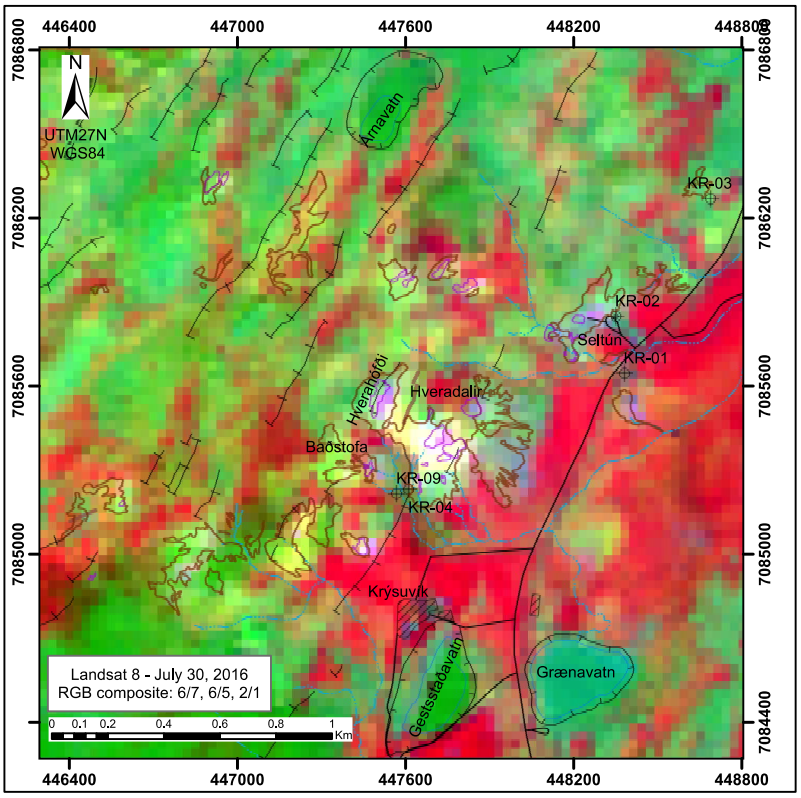

Figure 2. Band ratios 6/7,6/5,2/1 composite from Landsat 8 (July 30, 2016). Within the geothermal area the ratio 6/7 (associated to kaolinite and montmorillonite) seems to be widely spread and mixed with: sulphur, anatase, and covellite in magenta pixels; and with iron oxides like hematite and goethite in the yellow pixels.

Figure 3 displays the PCA for Landsat 5 from September 15, 1998, using the Crosta technique and the F, H+F,H composite [8]. From the map, red pixels within the geothermal area represent the iron absorption (F), interpreted as possible hematite and goethite, dark blue pixels represent the hydroxyl

absorption (H) and are interpreted as possible montmorillonite and kaolinite; orange and cyan represent a mixture where, in the first case, the iron absorption dominates, and in the second case the hydroxyl absorption dominates.

Figure 4 plots the wavelength positions of the main absorption features from Hyperion image from December 2, 2010. Just selected pixels within Hveradalir and Seltún were analysed. The wavelength positions are grouped into two spectral ranges: 0.671 to 1.500 µm and 1.500 to 2.224 µm, corresponding to the NIR and SWIR respectively. In general, iron oxides will have absorption features dominated by electronic processes in the VIS and NIR, while the absorption features in the SWIR are related to vibrational processes where H_2O, OH^- and CO_3^{-2} are present [9].

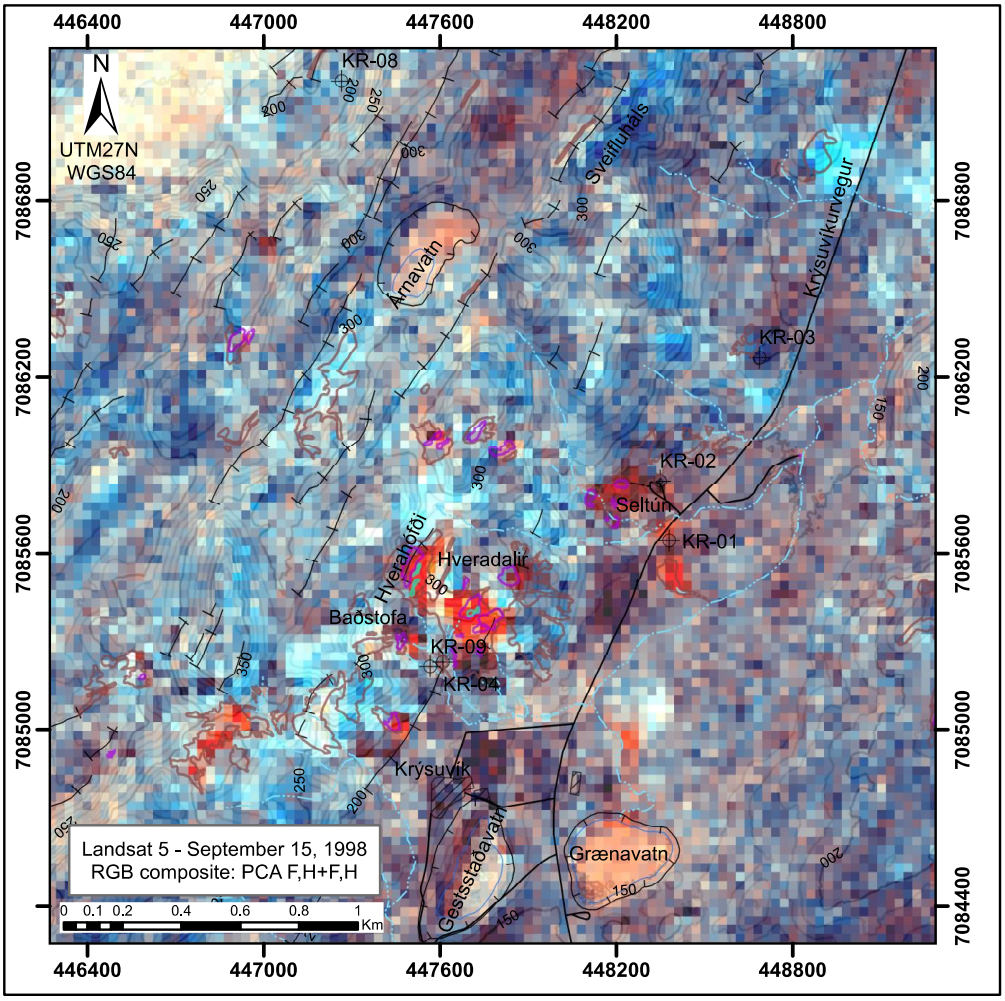

Figure 3. PCA-F,H+F,H composite from Landsat 5 (September 15, 1998). Red pixels represent iron absorption (F), and dark blue hydroxyl absorption (H).

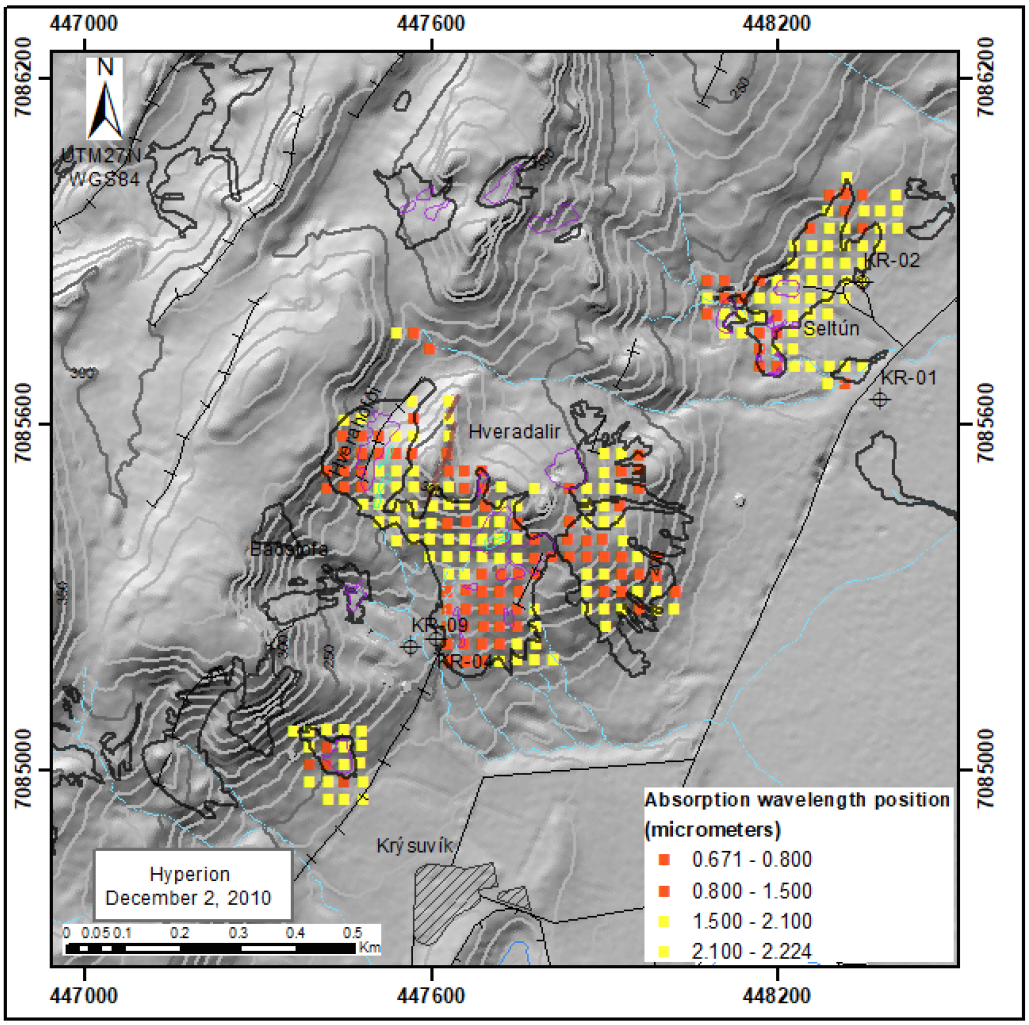

Figure 4. Wavelength position of the main absorption feature from Hyperion (December 2, 2010).

Figure 5 shows the time series of thermal anomalies from 2002 to 2017 by using Landsat and ASTER nighttime images. Thermal anomalies go from 2 standard deviations (SD) above the background (BG) temperature in yellow, to more than 6SD>BG in red. The BG temperature is shown in grey.

Thermal anomalies seem to be largely consistent within the geothermal area over the time. However, there is a thermal anomaly at the southeast of the study area that is not detected on September 22, 2010 and November 12, 2011 (marked with purple in Figure 5). Those dates are close to the beginning and the end of a change in trend of the vertical component detected by CGPS stations around Krýsuvík (Figure 6). Around that time, there is a reported uplifting period [13]. The absence of the thermal anomaly can be related to the peaks of the deformation trend. Further studies for that specific area are needed for better interpretation. The thermal anomaly in Seltún on September 22, 2010 is not detected because of a cloud covering that area. Differences among all the maps for thermal anomalies of 2SD>BG can be related to the different seasonal acquisition time.

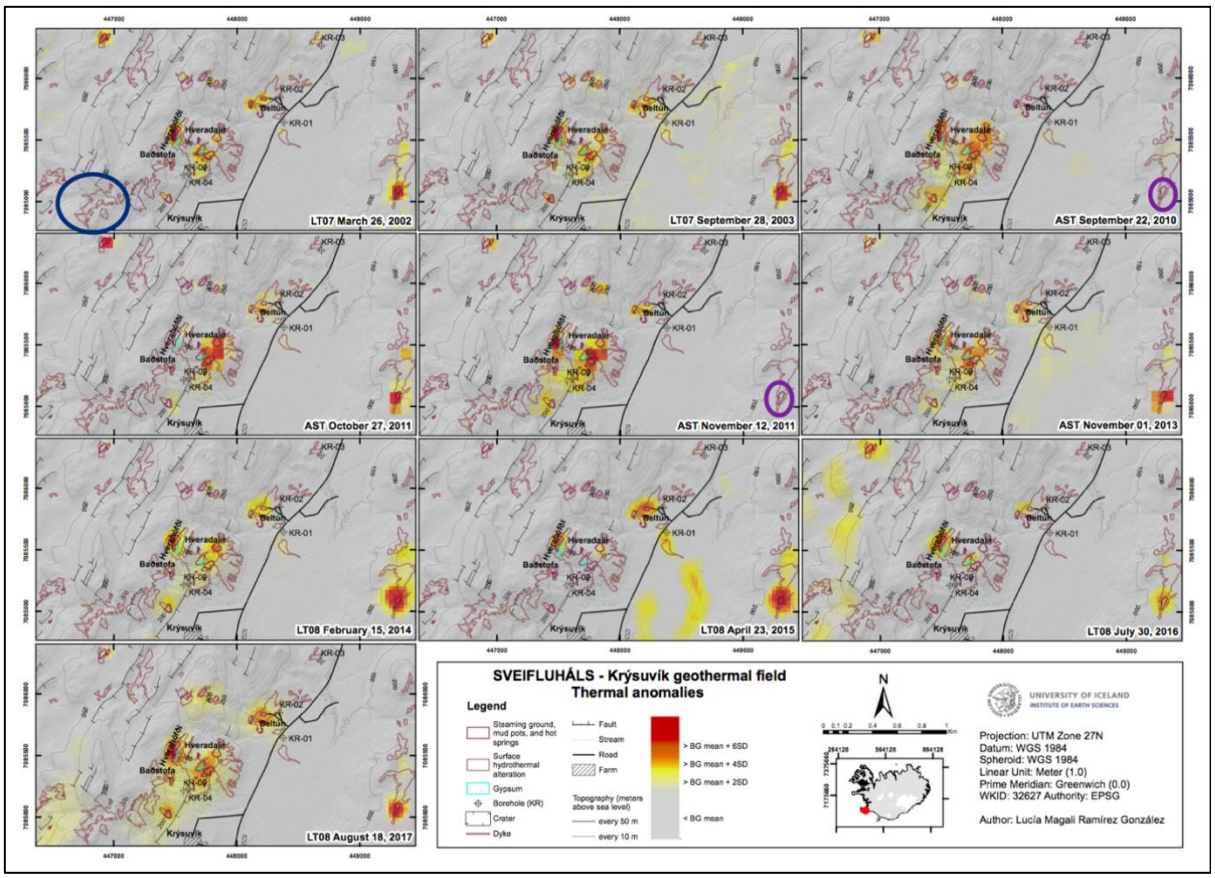

Figure 5. Thermal anomalies over the Sveifluháls sub-geothermal field. Thermal anomalies were categorized by standard deviations (SD) above the background (BG) temperature. LT and AST are for Landsat and ASTER respectively. Within purple oval the thermal anomaly possible affected by crustal deformation. Blue oval shows the area where hydrothermal alteration was identified but no thermal anomalies are currently noted.

Figure 5 also shows a zone at the southwest of the study area where hydrothermal alteration was identified but no thermal anomalies are noted, at least since 2002. This zone is marked within the blue oval in Figure 5 for the first image but the same lack of thermal anomaly prevails for all the images. This observation reveals that the zone had thermal anomalies in the past but not anymore. This could be related for example to cooling of that part of the field, clogging of the fractures or changes in the water table level. Further studies are needed for better interpretation.

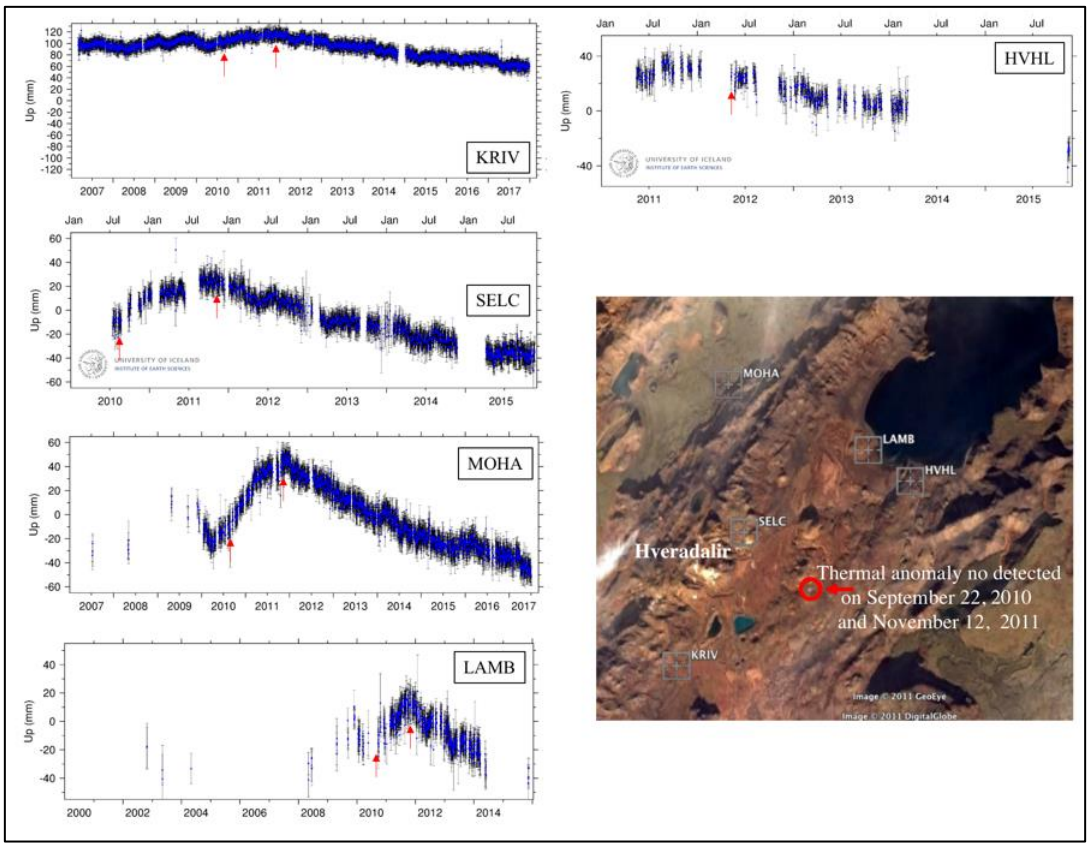

Figure 6. Time series of vertical displacements detected by CGPS around Krýsuvík. The red arrows are located on September, 2010, and November 2011. The stations belong to the Institute of Earth Sciences of the University of Iceland.

Regarding the TIR images acquired by using the UAV, once the images were georeferenced and in degrees Celsius, the pixel temperature values were extracted from the same points where the ground measurements were taken. Then, those values were plotted against the ground measurements at 1 cm deep and the water of the fumaroles. The depth of 1 cm is because of it corresponds to the tip of the temperature probe where the measurements are taken, and can be acceptably comparable with the surface temperature obtained from the thermal camera. The plots (Figure 7) show a linear relationship at all altitudes. The linear regression equations were fitted by using Microsoft Excel and those equations were used to calibrate the thermal images. The coefficient of determination (R^2) for the linear regressions was about 0.95 for TIR images taken from 10 m to 30 m high and decreased with altitude of the camera to reach 0.77 at the 100 m high image. The highest temperatures that correspond to the water of the fumaroles, increase dispersion by increasing the elevation. This makes sense because of the water of the fumaroles covered a small area, so, due to the fixed field of view (FOV) of the camera, by increasing elevation, the pixel size increases and the temperature of the pixel becomes integrated (average temperature within the pixel).

Heat flux estimation was done by using the TIR image taken from elevation of 30 m. This image was chosen because it covers all the points where the ground measurements were taken and because of its high R^2 value.

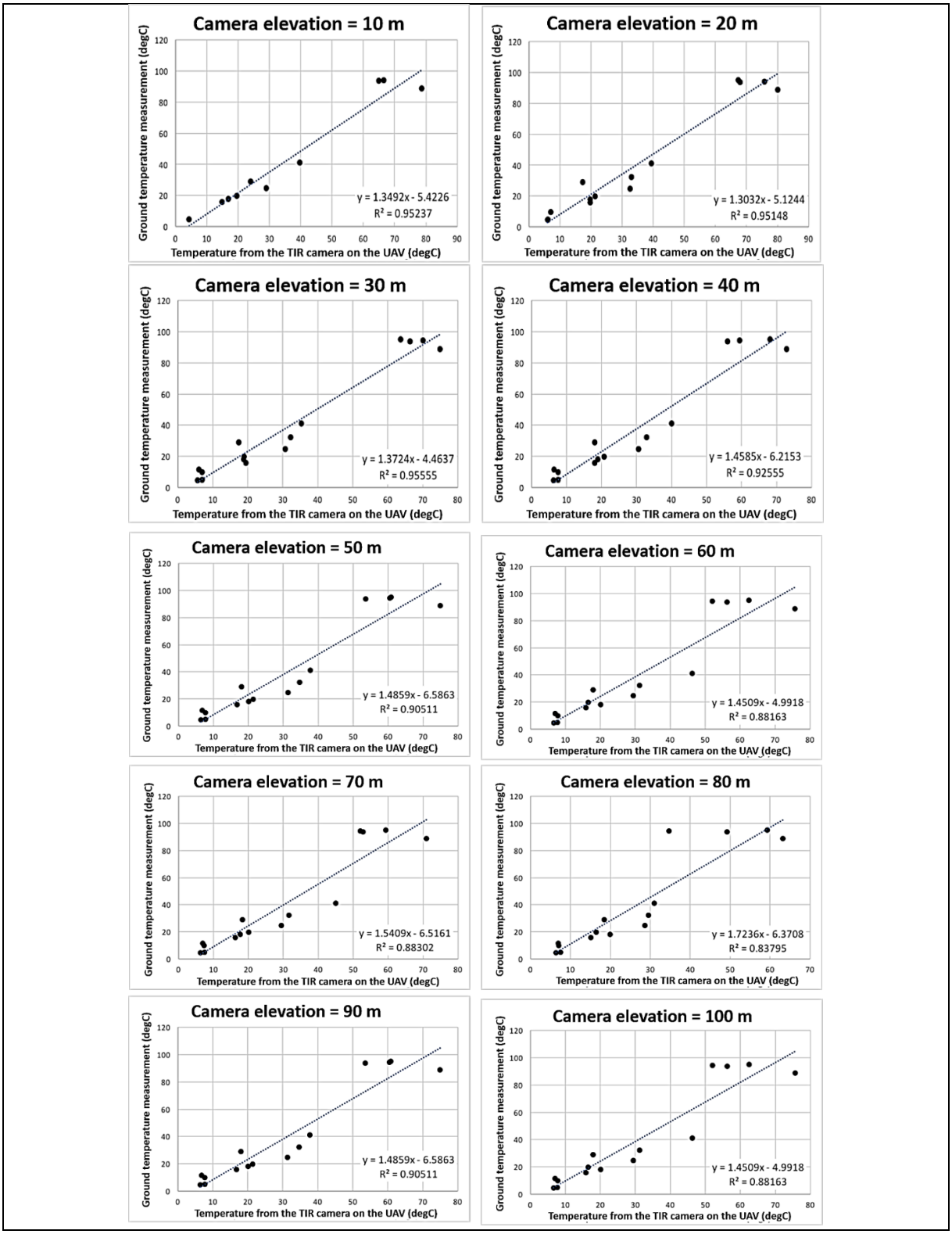

Figure 7. Plots of temperatures extracted from the TIR images acquired by the camera on the UAV at different altitudes vs. ground temperature measurements of water and soil at 1 cm deep. Linear regression equations and R^2 are also displayed.

In this way, the thermal radiant loss or the instant radiated thermal power was calculated for the pixels of the calibrated thermal image (in Kelvin) (Figure 8) using the equation (1) where 1.39 x10^{-3} m^2 was the pixel area. Then, the thermal radiant loss of the pixels contained within the isotherm of 6.35 °C (279.5 K) were summed up. This isotherm represents the main thermal anomaly. The obtained heat flux was 4.09 kW in an area of 102.5 m^2.

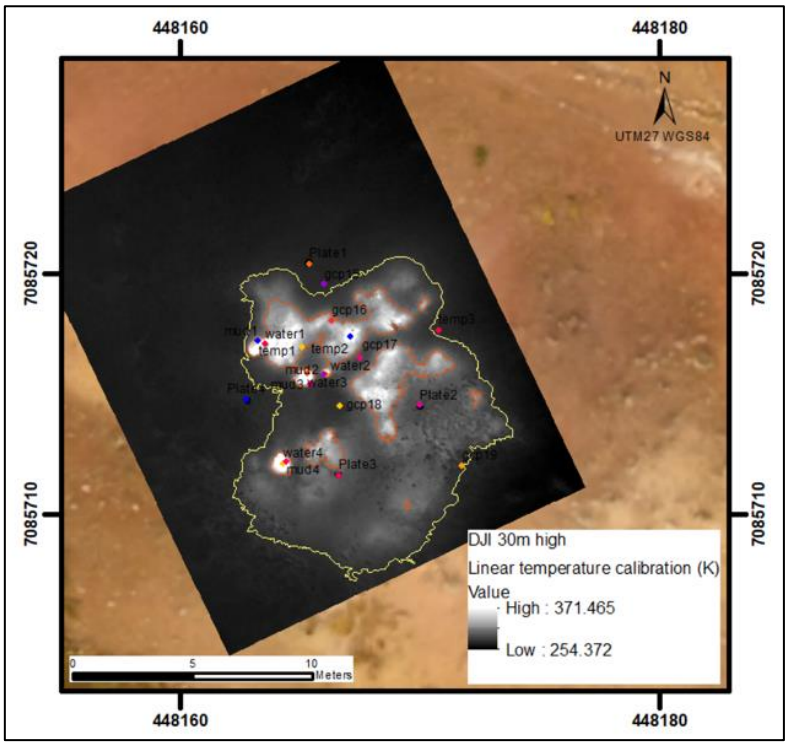

Figure 8. TIR image taken from elevation of 30 m, calibrated by its linear regression equation and in Kelvin. The pixel values were used for estimation of the heat flux by radiation. The red and yellow lines surrounding the thermal anomalies correspond to the isotherms of 13.95°C and 6.35 °C respectively and were used as reference for the calculation of heat flux through the soil. The colored dots are where the ground measurements were taken.

With the ground temperature measurements, the heat flux density through the soil was obtained by the method of Dawson (1964) (2). Then, the heat flux density value of each point was classified according to its position within the isotherms of 6.35 °C and 13.95 °C. So, heat flux density values within the 6.35 °C isotherm but out of the one of 13.95 °C, were averaged and multiplied by the area of 82.23 m^2, while heat flux values within the 13.95 °C isotherm were averaged and multiplied by 20.24 m^2. The total heat flux through soil was 5.17 kW in 102.5 m^2. Heat flux value obtained by using the TIR images, and the value obtained by using the ground measurements are of the same order of magnitude.

As reference Figure 9 shows the area covered by the 30 m high TIR image taken by the UAV (dark rectangle) and how the area is seen by the Landsat and ASTER satellite based sensors. For Landsat and ASTER, the area belongs to a pixel which thermal anomaly is around 2SD>BG. Given the size of the hot spots, the use of the UAV data was an important key for heat flux estimation; at the spatial resolution of the satellite images it is not effectively solved.

The analysis of the satellite images enabled us to categorize the geothermal activity in Sveifluháls. The results show that three groups of spectral signatures can be recognized in the study area according to the position of the main absorption feature: absorption in the VIS, NIR and SWIR. Spectral signatures which main absorption is located in the VIS and NIR, match with thermal anomalies that are greater than 4SD>BG. Spectral signatures with absorption in the SWIR are widely distributed in the geothermal area, but they are dominant where thermal anomalies are around 2SD>BG. This arrangement can be grouped into three levels (Figure 10):

- High activity. Characterized by thermal anomalies 6SD>BG, and absorption in the VIS and NIR that can be interpreted as spectral signatures of sulfur and iron oxides. For those areas, all the geothermal surface manifestations are present, including hot springs, steaming ground, fumaroles, and mud pots.

- Medium activity. Thermal anomalies are 4SD>BG, the spectral analysis suggests a mixture of minerals with absorption in the NIR and SWIR, but the NIR predominates. This can be associated to iron oxides like hematite and goethite. Those areas host small fumaroles and hot ground.
- Low activity. The thermal anomalies are 2SD>BG mainly because of warm ground. Spectral signatures show absorption in the SWIR and can correspond to montmorillonite.

Gypsum is a mineral mapped in all previous studies. However, its spectral signature can be confused with other minerals when using multispectral satellite images. In the case of kaolinite, its spectral signature is very similar to montmorillonite and in this study it was not possible to distinguish between them. However according to the description of the previous geochemistry study [7], the occurrence of kaolinite is associated to high activity and montmorillonite to low activity areas. Thus, the SWIR absorption can be attributed to kaolinite in areas of high thermal anomalies, and to montmorillonite in areas of low thermal anomalies. The use of hyperspectral data can help to solve those minerals, so it is suggested the use of hyperspectral cameras mounted on planes or UAVs, or the use of portable hyperspectral remote sensors that allow the discrimination of those minerals by remote sensing.

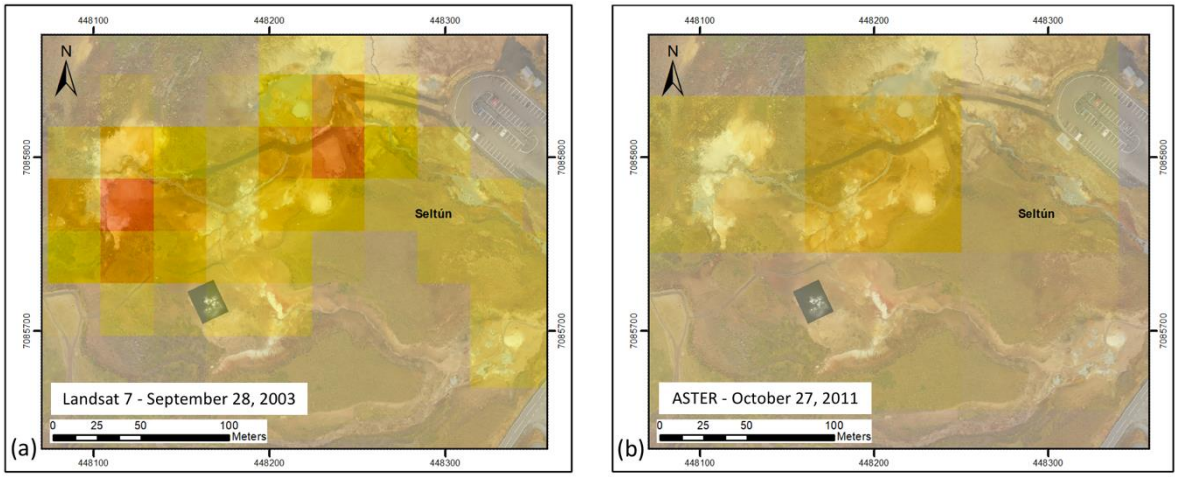

Figure 9. Comparison between spatial resolutions. The dark rectangle represents the area covered by the TIR imagen from the elevation of 30 m with the UAV. The yellow squares are the 2-4SD>BG thermal pixels from Landsat (a) and ASTER (b).

4. Concluding remarks

Based on the wavelength position of the main absorption feature from the multispectral and hyperspectral satellite images, three groups of spectral signatures can be recognized within the Sveifluháls-Krýsuvík geothermal area: absorption in the VIS, NIR and SWIR. Specific minerals for each group can be proposed/interpreted by using geochemistry analysis as reference. Absorption in the VIS and NIR were interpreted as sulfur and iron oxides like hematite and goethite and they were found in areas of thermal anomalies more than 4 SD above the background temperature. Absorption in the SWIR was interpreted as spectral signature of montmorillonite in areas of thermal anomalies 2 SD above the BG.

The kinetic LST retrieved from the TIR bands of Landsat and ASTER allowed a time series analysis of thermal anomalies from 2002 to 2017. The analysis showed consistent spatial distribution of the thermal anomalies in the study area. This time series of thermal anomalies revealed a zone at the southeast of the study area where thermal anomalies were not detected on September 22, 2010 and November 12, 2011. Those dates match with the beginning and the end of an uplifting period detected by the CGPS stations around Krýsuvík. Further studies of seismicity and crustal deformation for that specific area are needed for better interpretation. The analysis of thermal anomalies also detected a zone at the southwest of the study area where hydrothermal alteration was identified but no thermal anomalies

are currently noted. This can be related to cooling of that part of the field, clogging of the fractures or changes on the water table level; further studies are needed.

The use of the high spatial resolution TIR images taken from a UAV allowed detailed thermal analysis on Seltún. Radiation heat flux calculated using the TIR image taken at 30 m elevation gave 4.091 kW over an area of 102.5 m^2; same order of magnitude than the heat flux through the soil estimated by using ground temperature measurements. Detailed mapping of thermal anomalies and heat flux estimations using TIR cameras on UAV can give reliable results if the TIR images are acquired and processed properly. Flights at 30 m of elevation seem to be appropriate.

This study demonstrates that the combination of processing techniques, the use of sensors with different spectral and spatial resolution, as well as using images with different acquisition dates, allows regional and local analysis of the surface manifestations in a geothermal field. This study provides insights for monitoring natural or induced changes on the surface geothermal activity in other geothermal fields.

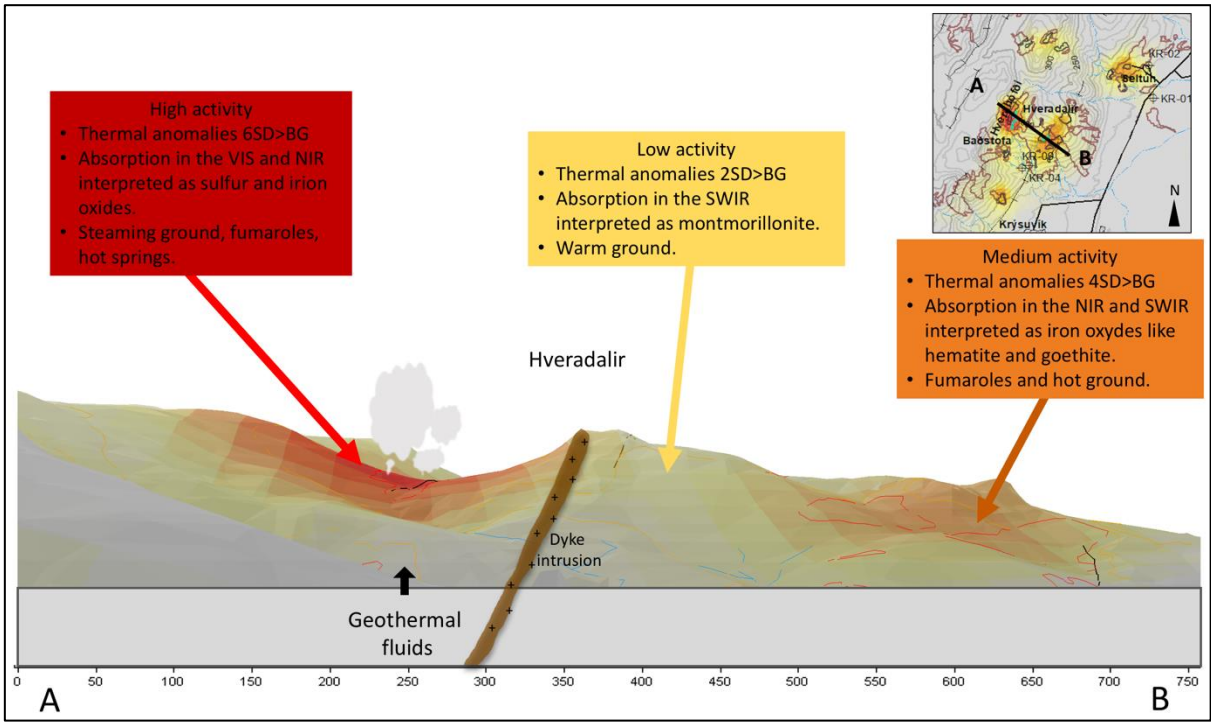

Figure 10. Schematized cross section over Hveradalir. The three proposed activity levels are shown. The section shows the topography of the area but is off-scale. The dyke intrusion is inferred from previous maps [3,5].

References

[1] Einarsson S Vogfjörd K Ilyinskaya E Oddsson B Pagneux E 2015 The Krysuvík-Trölladyngja volcanic system In:Ilyinskaya, Larsen and Gudmundsson (eds.): *Cataloge of Icelandic Volcanoes.* IMO, UI, CPD-NCIP.

[2] SAMSÝN Aerial photographs retrieved February 2017 from http://www.samsyn.is

[3] Khubaeva O 2007 Geothermal mapping in the Krýsuvík geothermal field *United Nations University - Geothermal Training Programme* Report **8** 2007 145-156.

[4] Mawejje P 2007 Geothermal Exploration and Geological Mapping at Seltún in Krýsuvík Geothermal Field, Reykjanes Peninsula, SW-Iceland *United Nations University - Geothermal*

Training Programme Report **12** 2007 257-276.
[5] Orkustofnun 2015 R3266A Sveifluháls, Krísuvík (in Icelandic) Orkustofnunar HS Orka report OS-2015/04.
[6] Chavez P S 1988 An improved dark object subtraction technique for atmospheric scattering correction for multispectral data *J. Remote sensing of Environment* **24** 459-479.
[7] Markússon S H and Stefánsson A 2011 Geothermal surface alteration of basalts, Krysuvik Iceland-Alteration mineralogy, water chemistry and the effects of acid supply on the alteration process *J. of Volcanology and Geothermal Research* **206** 46–59.
[8] Loughlin W P 1991 Principal Component Analysis for Alteration Mapping *Photogrammetric Engineering and Remote Sensing* **57** 1163-1169.
[9] Van der Meer F 2004 Analysis of spectral absorption features in hyperspectral imagery *Int. J. of Applied Earth Observation and Geoinformation* **5**, 55-68.
[10] Kealy P S and Hook S K 2013 Separating Temperature and Emissivity in Thermal Infrared Multispectral Scanner Data: Implications for Recovering Land Surface Temperatures *IEEE Transactions on Geoscience and Remote Sensing* Vol **31** (6)
[11] Dawson B 1964 The nature and assesment of heat flow from hydrothermal areas *New Zealand J. of Geology and Geophysics* **7** 155-171.
[12] Fridriksson T Kristjánsson B Ármannsson H Margrétardóttir E Ólafsdóttir S and Chiodini G 2006 CO_2 emissions and heat flow through soil, fumaroles, and steam heated mud pools at the Reykjanes geothermal area, SW Iceland *Applied Geochemistry* **21** 1551-1569.
[13] Michalczewska K Hreinsdóttir S Árnadóttir Th Hjaltadóttir S Ágústsdóttir Th Gudmundsson M T Geirsson H Sigmundsson F and Gudmundsson G B 2012 The inflation and deflation episodes in the Krísuvík volcanic system. Abstract ID: V33A-2843, *AGU Fall Meeting, December 2012*.